8

Upper atmospheres of the giant planets

LUKE MOORE, TOM STALLARD, AND MARINA GALAND

All celestial bodies are surrounded by gaseous envelopes, at least to some degree. When the gas is gravitationally bound to a parent body's nucleus it is called an atmosphere, whereas if the gas is not confined by gravity, such as at a comet, it is called a coma (Strobel, 2002). At one atmospheric extreme, such as Mercury or the Moon, the extremely tenuous atmosphere originating from the surface is referred to as a surface-bound exosphere, as the atmospheric atoms and molecules are much more likely to escape to space or to collide with the surface rather than collide with each other. At the other extreme, such as at the gas giants (Jupiter, Saturn, Uranus, Neptune), the rocky core about which the atmosphere is gravitationally bound is on the order of 0.1 planetary radii and gas constitutes the majority of the planet. A dense atmosphere is typically divided into two broad categories: the lower and upper atmospheres. The study of the lower regions (troposphere and stratosphere) forms the discipline of meteorology, while the study of the upper regions (mesosphere, thermosphere, exosphere) and their ionized component (ionosphere) forms the discipline of aeronomy.

Atmospheres play vital roles in planetary and satellite evolution, as they help to insulate the surface of a body from external influences. In particular, the upper atmosphere represents a key transition region between a dense atmosphere below and a tenuous space environment above. An array of complex coupling processes from below, such as waves, and from above, such as forcing by solar extreme ultraviolet (EUV) photons and energetic particles, means that aeronomy deals with the highly coupled system of neutrals, plasmas, and electromagnetic processes that link planets, moons, and comets from their surfaces to their magnetospheres, to the solar wind, and ultimately to the Sun itself (Mendillo *et al.*, 2002).

Evidence of these coupling processes include various upper-atmospheric emissions, such as dayglow and nightglow, resulting from the absorption of solar photons, and aurorae, which are produced by the energy deposition of energetic particles from the space environment. Such emissions can be detected remotely,

and have consequently allowed detailed study of the planets in the solar system. In addition to a host of ground-based observations, a number of spacecraft have also been used to study the giant planets. Spacecraft encounters with the outer planets include Pioneer 10 and 11 in the 1970s, Voyager 1 and 2 in the 1970s and 1980s, and New Horizons at Jupiter in 2007. More in depth studies have also been enabled by orbiting spacecraft: Galileo at Jupiter (1995–2003) and Cassini at Saturn (starting in 2004). The coupled atmosphere–magnetosphere systems at the giant planets are smaller scale representations of electromagnetic interaction regions that occur elsewhere in the universe. Furthermore, many hot Jupiters and hot Neptunes have been discovered so far (see Ch. 5; also, e.g., Fogg and Nelson, 2007; McNeil and Nelson, 2010), and by studying the giant planets in our own neighborhood we can improve our understanding of the rapidly accumulating zoo of exoplanets.

Much of early outer planet science was guided by our knowledge of the terrestrial system. Now, following nearly 40 years of spacecraft exploration and continually improving Earth-based capabilities, we understand enough about the giant-planet atmosphere–magnetosphere systems to categorize them based on the different processes that dominate each. Such a comparative approach has proven to be beneficial for study of all of the solar system planets, and will serve as a useful platform for initializing study of exoplanets and furthering our understanding of planetary formation and evolution. Subtle differences in atmospheric composition, magnetic field, internal magnetospheric plasma sources, and external forcing have led to significant differences in atmospheric and auroral morphology and dynamics at Jupiter, Saturn, Uranus, and Neptune. Similar exciting differences can be expected at other Jupiter-like exoplanets, in addition to the differences in stellar forcing. The future of comparative aeronomy is likely to be an exciting and enriching one.

In this chapter we give an overview of the current state of knowledge of giant-planet upper atmospheres (an overview of terrestrial upper atmospheres follows in Ch. 9). We focus first on the thermosphere and ionosphere, next on the processes coupling planetary atmospheres and magnetospheres, and finally on the auroral emissions resulting from those coupling processes. In addition to the references cited herein, further basic concepts are explored in more detail in related review chapters in the Heliophysics series (cf., Table 1.2), such as in Vol. I, Ch. 12, in Vol. III, Ch. 13, and in Ch. 9 in this volume for upper atmospheres, and in Vol. I, Chs. 10, 11, and 13, and Vol. II, Ch. 10 for magnetospheres.

8.1 Thermospheres of the giant planets

The atmospheres of the solar system giant planets are predominantly molecular hydrogen and (mostly inert) helium. Consequently the resulting photochemistry

differs significantly from other classes of atmospheres, such as the N_2-dominated atmospheres of Earth, Pluto, and Titan, or the CO_2-dominated atmospheres of Venus and Mars. Trace amounts of heavier cosmically abundant elements are also present in the deep atmospheres of the giant planets, though primarily in the form of hydrides due to the profusion of hydrogen (e.g., CH_4, NH_3, H_2O, H_2S, etc.). While turbulent (or eddy) diffusion acts to mix atmospheric constituents in the lower atmosphere (referred to as the homosphere) and thereby maintain constant vertical mixing ratios, there is a transition region – called the turbopause or homopause – above which less frequent collisions allow molecular diffusion to dominate and atmospheric constituents begin to separate according to their masses (a region referred to as the heterosphere). At the giant planets, the lower atmosphere includes a minimum in temperature with a negative temperature gradient in the troposphere and a positive gradient in the stratosphere. The upper atmosphere, primarily within the heterosphere, is characterized by a positive temperature gradient due to the absorption of EUV solar radiation and energy deposition from above and below. This region can further be separated into two coincident fluid components – the charged ionosphere and the neutral thermosphere – beneath a mixed kinetic component, the exosphere. While atmospheric species are still largely gravitationally bound within the exosphere, collisions are too infrequent to lead to a collective fluid behavior. It is a region where escape occurs and it is associated with a roughly isothermal temperature referred to as the exospheric temperature. The upper atmosphere, therefore, represents the boundary between a dense atmosphere below and a magnetosphere above, and mediates the exchange of particles, momentum, and energy between these two regions.

Dominant atmospheric constituents at the homopause of giant planets are molecular hydrogen, helium, and methane (CH_4). Above the homopause methane and other hydrocarbons are quickly separated out due to their relatively high masses and confined to the lower portions of the upper atmosphere; the atomic hydrogen fraction consequently continually increases with altitude. Therefore, while there is a complex array of hydrocarbon chemistry at work in the giant-planet atmospheres, it is primarily important for the formation of clouds, hazes, and aerosols in the lower atmosphere, leaving hydrogen photochemistry to dominate over the majority of the upper atmosphere. Despite the apparent simplicity of having one atmospheric constituent dominate the chemistry of a region there are a number of observations of giant-planet upper atmospheres that have yet to be explained by theory, including global thermal structure and ionospheric variability.

Measurements of giant-planet thermospheric properties are typically made remotely using occultations in the ultraviolet (UV), infrared, and radio spectral regions (visible occultation observations are hampered by the bright background of reflected solar light; radio occultation is described in Ch. 13). Jupiter is unique

Table 8.1 *Planetary and atmospheric properties for the gas giants*

	Jupiter	Saturn	Uranus	Neptune
Mass ($\times 10^{27}$ kg)	1.9	0.57	0.087	0.10
R_{eq} ($\times 10^3$ km)	71.5	60.3	25.6	24.8
R_{pole} ($\times 10^3$ km)	66.9	54.4	25.0	24.3
Day (Earth hours)	9.925[a]	10.656[b]	17.24	16.11
Year (Earth years)	11.86	29.24	83.75	164.7
Semi-major axis (AU)	5.20	9.58	19.2	30.0
Obliquity (°)	3.13	26.73	97.77	28.32
Dipole moment ($\times 10^{17}$ T m^3)[c]	1600	47	3.8	2.8
Dipole tilt (°)	9.6	<0.1	58.6	46.9
Dipole offset (R_{planet})	0.13	0.04	0.30	0.55
T at 1 bar (K)	165	134	76	72
T at homopause (K)	176	160	~200	~250
T at exobase (K)	900	420	800	750
Atmospheric composition by volume				
H_2	89.8%	96.3%	82.5%	80.0%
He	10.2%	3.25%	15.2%	18.5%
CH_4	3000 ppm	4500 ppm	2.3%	1.5%
Energy input (GW) from EUV photons and from precipitating particles[d]				
Photons: solar EUV	800–1200	150–270	8	3
Precipitating particles: auroral	10^5	10^4	100	1

[a] System III (1965) spin period of 9h 55m 29.711s (e.g., Bagenal *et al.*, 2014).
[b] Saturn's rotational period is not as well defined (e.g., Hubbard *et al.*, 2009; Read *et al.*, 2009).
[c] Schunk and Nagy (2009).
[d] Strobel (2002); Cowley *et al.* (2004); Müller-Wodarg *et al.* (2006).
Most tabulated values are from NASA Planetary Fact Sheets: http://nssdc.gsfc.nasa.gov/planetary/planetfact.html.
Occultation references: Jupiter: Eshleman *et al.*, 1979; Atreya *et al.*, 1981; Broadfoot *et al.*, 1981; Festou *et al.*, 1981; Hubbard *et al.*, 1995; Yelle *et al.*, 1996; Hinson *et al.*, 1997, 1998; Saturn: Festou and Atreya, 1982; Smith *et al.*, 1983; Lindal *et al.*, 1985; Hubbard *et al.*, 1997; Koskinen *et al.*, 2013; Uranus: Herbert *et al.*, 1987; Lindal *et al.*, 1987; Neptune: Broadfoot *et al.*, 1989; Lindal, 1992.

among the giant planets in that the Galileo Probe also made in situ atmospheric measurements (Seiff *et al.*, 1998). Stellar and solar UV occultations use the variation in the transmission of starlight/sunlight – as seen by an observer passing behind the planet – to derive the altitude profile of horizontal column density, which can be converted to an H_2 pressure–temperature profile by applying the ideal gas law ($p = \rho kT/m = nk_BT$) and hydrostatic equilibrium ($dp/dz = -\rho g$) assumptions (for a review see Smith and Hunten, 1990). In the preceding equations, p, ρ,

n, m, and T are the pressure, mass density, number density, mean molecular mass, and temperature of H_2, respectively; and z, g, R, and k_B represent altitude, gravity, the universal gas constant, and the Boltzmann constant, respectively. Longward of 110 nm, hydrocarbon species are the primary absorbers in giant-planet upper atmospheres, and so CH_4 mixing ratios and the homopause location can also be derived from UV occultations. Infrared ground-based stellar occultations can probe the lower thermospheres of giant planets by measuring the attenuation (via defocusing) of starlight caused by atmospheric refractivity gradients (e.g., Hubbard *et al.*, 1995). Similarly, radio occultations track the diminution of a signal emitted by a spacecraft and measured by a radio telescope at Earth. The refractive defocusing of radio signals can be caused by the neutral atmosphere and by free electrons, and so radio occultations probe both lower atmospheric properties and ionospheric electron densities. A list of key references of giant-planet occultation observations is given in Table 8.1, along with basic planetary and upper-atmospheric properties.

Upper-atmospheric mixing ratios (Fig. 8.1), number densities, and temperatures (Fig. 8.2) have been derived from the Galileo Probe measurements at Jupiter; they are qualitatively representative of other giant-planet mixing ratios and thermal profiles. The Jovian homopause is clearly identifiable in both figures as the region where mixing ratios suddenly diverge from their constant lower atmospheric values (~350 km above the 1 bar pressure level). Figure 8.2 serves as a useful guide for basic thermospheric structure across all of the giant planets: e.g., the presence of methane and low temperatures near the homopause, and – in the upper atmosphere – the dominance of light species (H_2, H, and He) and a positive temperature gradient transitioning into an isothermal domain.

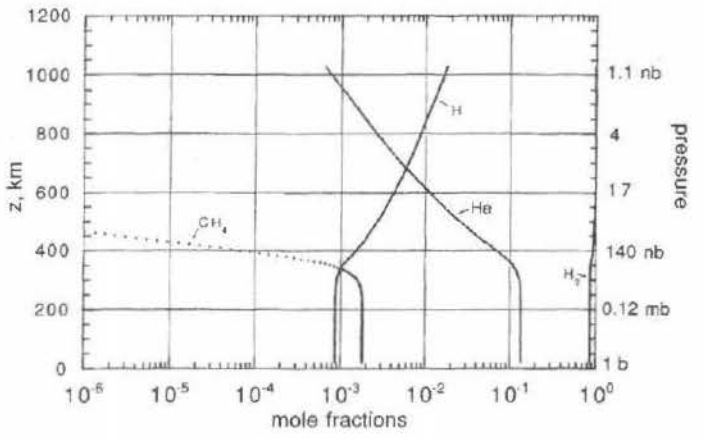

Fig. 8.1 *Galileo Probe* results showing Jupiter upper-atmospheric mixing ratios. Altitudes refer to radial distance above the 1 bar pressure level. (From Seiff *et al.*, 1998).

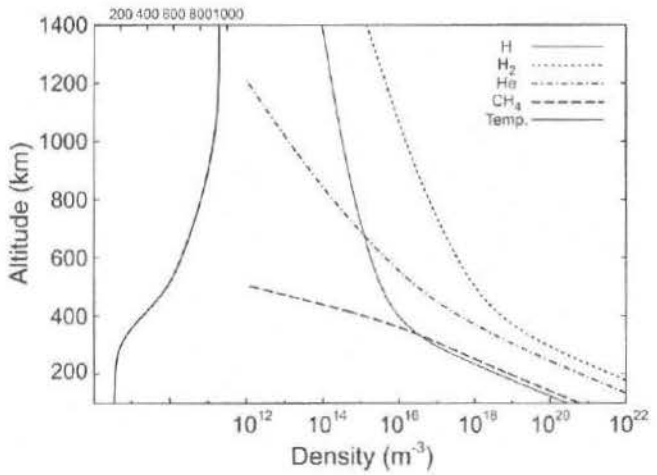

Fig. 8.2 Jupiter thermospheric parameters, based on *Galileo Probe* measurements. Altitudes refer to radial distance above the 1 bar pressure level. (From Barrow and Matcheva, 2011.)

Unlike at Earth, where the main energy source at non-auroral latitudes is usually solar radiation, the energy balance required to maintain the observed giant-planet thermospheric thermal structures at low- and mid-latitudes remains a puzzle. Possible sources of heating in giant-planet upper atmospheres include absorption of solar energy, precipitation of charged particles from the magnetosphere, and dissipation of kinetic energy in winds and waves. In general, absorption of solar EUV photons at thermospheric altitudes leads to downward heat conduction, generating a positive temperature gradient above the homopause. However, as illustrated in Fig. 8.3, calculations based solely on solar-energy inputs fall significantly short of reproducing the observed upper-atmospheric temperatures. Global solar EUV energy inputs at giant planets (e.g., ~1 TW and ~0.2 TW at Jupiter and Saturn, respectively), are dwarfed by magnetospheric energy inputs, estimated to be of order 10 TW or more (Miller *et al.*, 2005; Müller-Wodarg *et al.*, 2006). Consequently, the observed high temperatures at low latitudes may be related to a redistribution of energy inputs at auroral latitudes, though there remain significant problems with overcoming the powerful zonal winds generated by Coriolis forces on the rapidly rotating giant planets (e.g., Smith *et al.*, 2007; Müller-Wodarg *et al.*, 2012; see also Majeed *et al.*, 2005). Precipitation of charged particles can lead to heating primarily via the dissipation of energy resulting from currents in a resistive ionosphere. Commonly referred to as Joule heating, this process represents two components, the thermal heating of the atmosphere by electrical currents and the change in kinetic energy of the atmospheric gases which results from momentum change due to ion drag effects (Vasyliūnas and Song, 2005). The quantitative impact on giant-planet

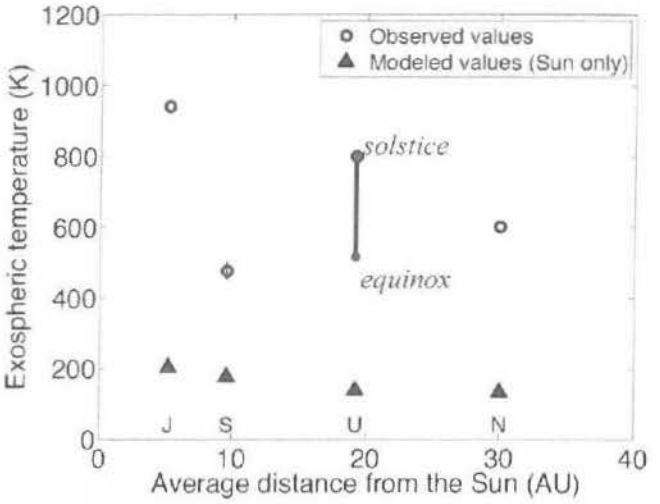

Fig. 8.3 Upper-atmospheric temperature as a function of heliocentric distance for the giant planets, comparing observations with model values using only solar irradiance as energy input (after Yelle and Miller, 2004; Melin *et al.*, 2011a, 2013). Note that these values represent a combination of measurements from a range of latitudes with different seasonal and solar conditions. In addition, the Uranus values include both neutral exobase temperatures as well as H_3^+ temperatures near the ionospheric peak altitude.

upper-atmospheric thermal structure of the third category of energy inputs – the dissipation of waves – remains unclear. Though Galileo Probe temperature measurements are consistent with upwardly propagating gravity waves (Young *et al.*, 1997), there is no consensus regarding their effects on thermospheric energetics (e.g., Matcheva and Strobel, 1999; Hickey *et al.*, 2000).

8.2 Ionospheres of the giant planets

Ionizing radiation at the giant planets comes primarily in two forms: solar EUV and soft X-ray photons, and energetic particle precipitation from the planetary magnetosphere, which is mostly concentrated at high magnetic latitudes. Roughly 90% of the ionizing radiation is absorbed directly by H_2, leading to the production of H_2^+ ions and electrons, usually suprathermal. These electrons, referred to as photoelectrons in the case of photoionization and secondary electrons in the case of particle impact ionization, possess enough energy to excite, dissociate, and further ionize the neutral atmosphere as well as to heat the ambient plasma. Therefore, in order to accurately model an ionosphere, it is necessary to track the evolution of both photons and electrons throughout the atmosphere. Photoionization production rates as a function of altitude and wavelength follow from application of the Lambert–Beer

Law assuming neutral atmospheric densities, incident solar fluxes, and photoabsorption and photoionization cross sections are known (see also Ch. 12 in Vol. I). The Lambert–Beer Law, also known as Beer's Law, the Beer–Lambert Law, or the Beer–Lambert–Bouguer Law, describes the attenuation of light through a medium (Houghton, 2002). In order to track the transport, energy degradation, and angular redistribution of suprathermal electrons – including photoelectrons as well as secondary electrons – a kinetic approach is typically applied by solving the Boltzmann equation (e.g., Perry *et al.*, 1999; Moore *et al.*, 2008; Galand *et al.*, 2009). The ion-production rates and thermal-heating rates generated by energetic electrons are dependent upon the ambient atmospheric parameters, which themselves are altered by the electron-energy deposition, and so iteration between atmospheric fluid and kinetic codes is required to close the solution.

The dominant giant-planet ionospheric ions are H^+ and H_3^+, though their relative importance is mostly unconstrained at present and is likely to vary with a range of parameters, including season, solar flux, latitude, and local time. While the rapid production of H_2^+ is balanced by an equally rapid loss via charge exchange with H_2, producing H_3^+, the slow production of H^+ is offset by a very slow radiative recombination loss process and a short day. In fact, early giant-planet ionospheric modelers predicted H^+ would be completely dominant (e.g., McElroy, 1973; Capone *et al.*, 1977), a notion that was challenged only when measured electron densities from radio occultations were found to be an order of magnitude smaller than predicted and to exhibit strong dawn/dusk asymmetries. This model–data discrepancy required the introduction of new photochemical loss chemistry that would reduce electron densities by converting long-lived atomic H^+ ions into short-lived molecular ions. Representative giant-planet ionospheric electron-density profiles derived from spacecraft radio occultation experiments are presented in Fig. 8.4. Ionization fractions at the giant-planet ionospheres are roughly of order 10^{-6}, smaller on average than ionization fractions in much of Earth's ionosphere (cf., Sect. 12.8 in Vol. I). In general, the EUV-driven peak electron densities near 1000 km decrease with heliocentric distance. Profiles shown in Fig. 8.4 are, however, associated with different solar conditions (solar activity, solar zenith angle) and magnetospheric conditions (e.g., particle precipitation).

The two additional most commonly suggested pathways for chemical loss of protons in giant-planet ionospheres are charge exchange with molecular hydrogen (McElroy, 1973) and charge exchange with water group and/or ice particles (Connerney and Waite, 1984). While the former – $H^+ + H_2(v \geq 4)$ – is exothermic only when H_2 is excited to the fourth or higher vibrational level, the latter – e.g., $H^+ + H_2O$ – depends on an external influx of water group particles such as H_2O or OH. Neither process is well constrained at present. There have been a few first-principles calculations of the vibrational levels of H_2 at Jupiter and Saturn (e.g.,

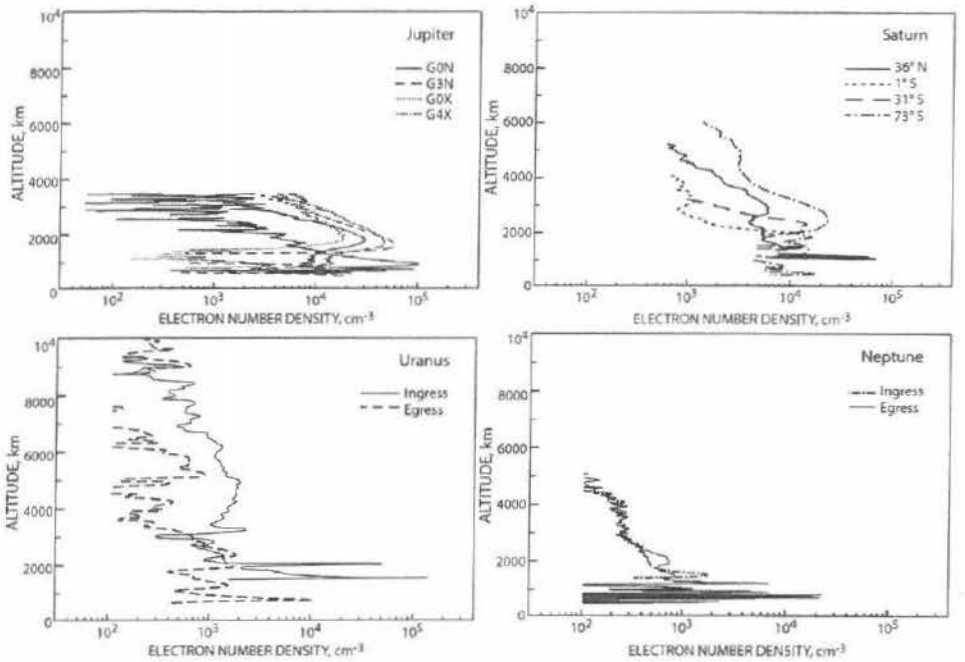

Fig. 8.4 Ionospheric electron-density profiles derived from spacecraft radio occultation experiments at (top left) Jupiter, (top right) Saturn, (bottom left) Uranus, and (bottom right) Neptune. Altitudes refer to radial distance above the 1 bar pressure level. Profiles are from the Galileo spacecraft for Jupiter (Yelle and Miller, 2004), and from the Voyager spacecraft for Saturn (Lindal *et al.*, 1985), Uranus (Lindal *et al.*, 1987), and Neptune (Lindal, 1992).

Cravens, 1987; Majeed *et al.*, 1991), but those estimates did not lead to consistent reproductions of observed electron densities. Consequently, contemporary models typically use some parametrization of those calculations in order to specify $H_2(v \geq 4)$ populations. Estimates of external particle influxes at the giant planets, on the other hand, are based primarily on Infrared Space Observatory observations of stratospheric carbon and oxygen bearing compounds (Feuchtgruber *et al.*, 1997; Moses *et al.*, 2000) and on electron density model–data discrepancies (e.g., Connerney and Waite, 1984; Moore *et al.*, 2010). Possible external sources of oxygen at all of the giant planets include direct atmospheric ablation of interplanetary dust particles, deposition of material following cometary impacts, and an influx of materials from rings or satellites. In particular, at Saturn, the water vapor plumes of Enceladus (Porco *et al.*, 2006) and the water ice rings imply ample sources of external water group particles are available (e.g., Tseng *et al.*, 2010; Fleshman *et al.*, 2012), and infrared observations of thermal H_3^+ emissions revealed a direct ring–atmosphere connection (Connerney, 2013; O'Donoghue *et al.*, 2013).

In addition to the major ionospheric ions, H^+ and H_3^+, giant-planet ionospheres are expected to exhibit an additional ledge of ionization above the homopause and below the ionospheric electron-density peak, initialized by charge-exchange reactions between the major ions and methane and also by direct photoionization of methane. This low-altitude ionospheric region is predicted to be dominated by hydrocarbon ions – wherein a complex array of hundreds of photochemical reactions culminates with ions such as $C_3H_5^+$ and CH_5^+ – and possibly also to play host to metallic ions derived from meteoroid ablation, such as Mg^+ (e.g., Kim and Fox, 1994; Moses and Bass, 2000; Y. Kim *et al.*, 2001, 2014). Narrow layers in electron density are observed frequently in and just above this region (Fig. 8.4), possibly caused by vertical shears in neutral winds (Lyons, 1995; Moses and Bass, 2000), such as might result from atmospheric gravity waves (Barrow and Matcheva, 2011). Similar electron density layers are also observed at other planets, such as sporadic-E layers at Earth (e.g., see Vol. III, Ch. 13). Vertical plasma drifts may also be behind the drastic variations in the observed altitudes of peak electron density (e.g., McConnell *et al.*, 1982). Sample model vertical ionospheric profiles that include various combinations of the above processes are shown in Fig. 8.5. Note that these model profiles are meant to be representative of the expected overall structure, and do not necessarily correspond to the specific conditions associated with the measured profiles shown in Fig. 8.4. However, by carefully specifying combinations of unconstrained parameters – such as oxygen influx, vibrational H_2 populations, and vertical plasma drifts – it is possible to reproduce much of the observed electron density structure.

Giant-planet low-altitude ionospheres (e.g., below ~600 km at Jupiter and below ~1000 km at Saturn), where hydrocarbon and H_3^+ ions dominate, are generally in photochemical equilibrium. The fast dissociative recombination rates of these molecular ions – tens of seconds to a few minutes – means that they are neutralized before any transport effects can have an impact, and consequently their densities can be derived directly from a series of ion continuity equations which balance ionization and chemical production with chemical loss. Assuming charge neutrality in a single ion component ionosphere (with $n_i = n_e$), photochemical equilibrium is represented schematically by $q = \alpha_{\text{eff}} n_e^2$, where q is the ion production rate, α_{eff} is the dissociative ion–electron recombination-rate coefficient (of order $\sim 10^{-7}\,\text{cm}^3\,\text{s}^{-1}$ for H_3^+ in giant-planet ionospheres), and n_e is the electron density. At higher altitudes – where dissociative recombination rates are slower due to reduced electron densities, and where H^+ charge-exchange loss processes are slow due to reduced neutral densities – ion transport plays an important role in determining ionospheric densities. Ion–neutral collision frequencies are much smaller than ion gyrofrequencies at high altitudes; consequently ions are primarily constrained to move along magnetic field lines, and so ion transport is modified

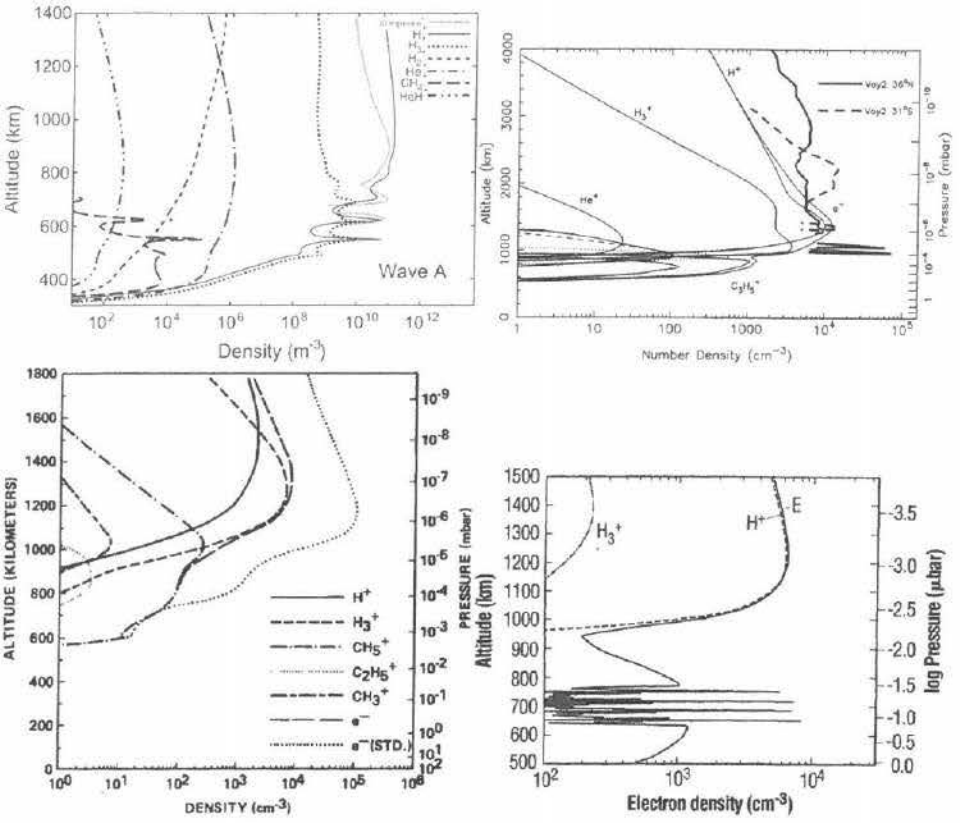

Fig. 8.5 Ionospheric model calculations for (top left) Jupiter, (top right) Saturn, (bottom left) Uranus, and (bottom right) Neptune. Altitudes refer to radial distance above the 1 bar pressure level. Note that electron density profiles are labeled as e^- in the Jupiter, Saturn, and Uranus panels, and as E in the Neptune panel. (Sources: Jupiter: Barrow and Matcheva, 2011; Saturn: Moses and Bass, 2000; Uranus: Chandler and Waite, 1986; Neptune: Lyons, 1995.)

by the planetary magnetic field. Ion-transport processes include drifts driven by neutral winds and ambipolar diffusion, wherein the electrical interaction between (relatively) heavy ions and nearly mass-less electrons leads to a coupled diffusion process and an ion scale height roughly twice that of the corresponding neutral.

Ionospheric structure at the giant planets is relatively unconstrained by observation. Radio occultations are sparse – with only nine published for Jupiter, 65 for Saturn, two for Uranus, and two for Neptune – and furthermore are all limited to measurements near the terminator, due to the geometry required by radio occultation observations of superior planets. Dawn and dusk are periods of rapid change in an ionosphere, as photoionization is turned on or off by the rising or setting of the Sun, and so are not ideal times to sample unknown ionospheric structure. At

Saturn, where the Cassini spacecraft (Jaffe and Herrell, 1997) has been in orbit since 1 July 2004, the increased number of radio occultation measurements has allowed identification of two main global ionospheric structures. First, there is a dawn/dusk asymmetry, with peak electron densities larger at dusk and the altitudes of the electron-density peak higher at dawn (Nagy *et al.*, 2006, 2009). Second, there is a counter-intuitive latitudinal behavior in electron density: peak electron densities are smallest at the equator – where solar ionization rates are largest – and increase with latitude (Kliore *et al.*, 2009). Both of these behaviors can be explained by an external oxygen influx from Saturn's rings and icy satellites, such as H_2O or O_2^+, if the influx maximizes at low latitude (e.g., Moore *et al.*, 2015).

Voyager and Cassini radio-wave measurements have also allowed a derivation of the diurnal variation in peak electron density at Saturn. Broadband radio signatures of powerful lower-atmospheric lightning storms, which for presently unknown reasons occur at only a select few latitudes, are refracted and attenuated by Saturn's ionosphere before being detected by a spacecraft. As the storm system rotates with the planet, the minimum measured Saturn Electrostatic Discharge (SED; note that this is a very different process from terrestrial storm enhanced densities for which the same acronym is used) frequency yields the peak electron density of the intervening plasma as a function of local time (Kaiser *et al.*, 1984; Fischer *et al.*, 2011). The strong diurnal variation in peak electron density derived from SED measurements has yet to be explained by models, however, as the ion production and loss rates implied by the observations are much larger than current best estimates (Majeed and McConnell, 1996; Moore *et al.*, 2012). No such similar emissions have been detected at the other giant planets, possibly due to a lack of active lightning discharge during spacecraft flybys, or to attenuation of the radio waves by the planetary ionospheres (Zarka, 1985), or to the slow nature of the lightning discharge itself (Farrell *et al.*, 1999).

One additional remote diagnostic of giant-planet ionospheres that has proven to be remarkably fruitful is the measurement of thermal H_3^+ emission in the infrared. First detected at Jupiter (Drossart *et al.*, 1989), it has since been observed regularly at Jupiter, Saturn, and Uranus, but not – so far – at Neptune. There are a number of strong H_3^+ rotational–vibrational emission lines available in the mid-IR, particularly in the L-band (3–4 micron) atmospheric window, and those emissions are strongly temperature dependent. Conveniently, this spectral region (e.g., near 3.4 micron) also corresponds to a deep methane absorption band, such that light from giant-planet interiors cannot escape, and H_3^+ emission therefore appears as bright emission against a dark background. Because H_3^+ is expected to be thermalized to the surrounding neutral atmosphere, it can be used to track both thermospheric temperatures and ionospheric H_3^+ column content. These factors combine to make H_3^+ an excellent probe of giant-planet upper atmospheres, and the fact that important emission lines fall within atmospheric transmission windows allows cost effective

observations from ground-based telescopes (see Miller *et al.*, 2010, and Stallard *et al.*, 2012b, for reviews).

Emission from giant-planet H_3^+ ions is strongest in the auroral regions, where particle precipitation enhances the local ionization far above solar-produced levels and where temperatures are largest. For this reason, a majority of H_3^+-related science has focused on understanding auroral structure and behavior. Giant-planet auroral UV emission is predominantly caused by inelastic collisions of energetic electrons with atmospheric molecular hydrogen, and represents a prompt response to changes in magnetospheric inputs. In contrast, auroral IR H_3^+ emissions represent the temporally integrated response of the upper atmosphere to those inputs above the homopause. Therefore, UV and IR emissions are highly complementary in studies of giant-planet auroral ionospheres (e.g., Melin *et al.*, 2011b; Radioti *et al.*, 2013). At Jupiter the hydrogen excitation aurora and the H_3^+ thermal aurora appear to be well separated in altitude (~250 km for the visible (Vasavada *et al.*, 1999) and ~1000 km for the IR (Lystrup *et al.*, 2008)) whereas at Saturn they peak at a similar altitude near 1150 km (in the UV; Gérard *et al.*, 2009; Stallard *et al.*, 2012a). No observational constraints are available at present regarding the altitude distribution of H_3^+ at Uranus or Neptune.

Though weak compared to auroral emissions, H_3^+ has also been detected across the dayside disk of Jupiter (Lam *et al.*, 1997), and the measured latitudinal variations indicate additional sources of non-solar mid-latitude ionization may be required (Rego *et al.*, 2000), though no magnetospheric source for this ionization has been suggested. Similarly, long-term H_3^+ observations have been made at Uranus – likely representing a range of combinations of auroral and non-auroral emission – revealing an unexplained cooling trend of the upper atmosphere, persisting past equinox (Melin *et al.*, 2013). At Saturn, the cooler thermospheric temperatures and the lower ionospheric densities meant that the prospect for observing non-auroral H_3^+ emission was slim. A low-latitude detection of H_3^+ made using the Keck telescope (O'Donoghue *et al.*, 2013), however, has reignited hopes of probing upper-atmospheric properties across the visible disk of Saturn. Even more intriguing, the O'Donoghue *et al.* measurements revealed significant latitudinal structure in H_3^+, with local extrema in one hemisphere being mirrored at magnetically conjugate latitudes, and mapping along magnetic field lines to regions of increased or decreased density in Saturn's rings, implying a direct ring–atmosphere connection (Connerney, 2013).

8.3 Ionosphere–thermosphere–magnetosphere and solar wind coupling

Particles, energy, and momentum are exchanged between planetary upper atmospheres and magnetospheres via currents that flow through the high magnetic latitude ionosphere. Birkeland currents, or currents which flow along planetary

magnetic field lines, supply angular momentum to the magnetosphere – by allowing closure of magnetospheric currents in the ionosphere – and energy – e.g., in the form of particle precipitation and associated Joule heating – to the atmosphere. Charged particles are accelerated into the atmosphere as a result of the varying charged particle density at different positions along planetary magnetic field lines. Both ions and electrons are concentrated in two locations, the ionosphere of the planet and close to the equatorial plane of the magnetosphere. There is, as a consequence, a lack of current-carrying plasma part-way along the field lines, particularly far from the magnetic equator, on the field line close to the planet above the exosphere. A circuit that closes through the ionosphere requires field-aligned potentials to develop in order to augment the electron distribution in this low-density region, allowing increased field-aligned currents to flow between the ionosphere and magnetosphere. The resultant current–voltage relation is nonlinear, depending upon the density and temperature of the electron population (Knight, 1973; Ray *et al.*, 2009). This acceleration of magnetospheric electrons not only increases the field-aligned current density, but also the energy and energy flux of the electrons precipitating into the atmosphere.

Ionospheric currents allow closure to the magnetospheric current system; they depend on local conditions, which are in turn strongly affected by the enhanced ionization brought by Birkeland currents. Electrical, ionospheric conductivities are associated with particle mobility in the direction perpendicular to the planetary magnetic field and parallel (Pedersen) or perpendicular (Hall) to the ionospheric electric field. Pedersen conductivities, associated primarily with a current carried by ions, peak in the lower ionosphere near the homopause, where the ion gyrofrequency is approximately equal to the ion–neutral collision frequency, and where molecular hydrocarbon ions begin to dominate. Hall conductivities, associated primarily with a current carried by electrons, peak at lower altitudes below the homopause, within a region of complex hydrocarbon chemistry. Pedersen and Hall conductances – or height-integrated conductivities – therefore depend upon local sources of ionization, ionospheric chemistry, and planetary magnetic field strength.

There are no direct observational constraints on ionospheric electrical conductances at the giant planets for a number of reasons. First, only roughly half of the relatively few electron-density altitude profiles retrieved from radio-occultation measurements extend down to the ionospheric conducting layers. Furthermore, there are no obvious auroral ionization signatures in the handful of high-latitude outer-planet radio occultations, therefore limiting their application to magnetosphere–ionosphere coupling studies. Second, the other main remote diagnostic of giant planet ionospheres – emission from H_3^+ – is a column integrated measurement, and therefore typically possesses little altitude information. To date H_3^+ altitude information has been derived only twice, once at Jupiter (Lystrup *et al.*, 2008) and once at Saturn (Stallard *et al.*, 2012a). Finally, even a

Table 8.2 *Pedersen conductances Σ_P calculated using energy deposition and ionospheric models and presented as a function of the ionization source (Sun, auroral electrons) over the main auroral oval. The characteristics of the auroral electrons are given in terms of the initial mean energy E_{prec} and energy flux Q_{prec}.*

Energy source [E_{prec} (keV), Q_{prec} (mW m^{-2})]	Pedersen conductance Σ_P (mho)	Reference [atmospheric model]
	Jupiter	
Electrons [10, 1]	0.04	
Electrons [10, 10]	0.12	Millward *et al.*, 2002
Electrons [10, 100]	0.62	[3D GCM]
Electrons [60, 10]	1.75	
Electrons [22, 100] and [3,10] and [0.1,0.5]	9 (NH)[a] 12.5 (SH)[a]	Bougher *et al.*, 2005 [3D GCM]
Electrons [1, 1]	0.008	Hiraki and Tao, 2008
Electrons [10, 10]	0.5	[1D ionospheric model]
	Saturn	
Solar only (Main oval: noon, 78°, equinox, solar minimum)	0.7	Galand *et al.*, 2011
Solar + Electrons [10, 1]	11.5	[1D ionospheric model
Solar + Electrons [10, 0.2]	5	using 3D neutral output]
Solar + Electrons [2, 0.2]	10	

[a] NH and SH stand for northern hemisphere and southern hemisphere, respectively.

complete H_3^+ altitude profile only provides a lower limit to the ionospheric conductance, as the dominant contribution from the hydrocarbon ion layer would still be missing. Therefore, in practice, ionospheric electrical conductances are commonly estimated from models – either magnetospheric models that require certain conductances to explain observations of magnetospheric phenomena (e.g., Cowley *et al.*, 2008) or ionospheric models which rely on assumed precipitation sources to calculate conductances from the resulting ionization (e.g., Millward *et al.*, 2002; Galand *et al.*, 2011).

Based on model calculations, ionospheric conductances are expected to be largest at low- and mid-latitudes on the dayside due to solar-induced ionization, and in the auroral regions at all local times due to particle precipitation. Additionally, outside of the auroral precipitation regions, where solar-induced ionization sources dominate, there are likely strong seasonal and local time variations corresponding to changes in the solar zenith angle. Table 8.2 summarizes some of the different estimates of ionospheric Pedersen conductances in the literature (which have only been made for Jupiter and Saturn thus far).

The variations between the Pedersen conductances derived for Jupiter and Saturn (Table 8.2) are driven primarily by differences in planetary magnetic field strength, affecting ion gyrofrequency, and the particle precipitation energies and fluxes. On the one hand, more-energetic particles deposit their energies at lower altitude within an atmosphere, and so there is a range of energies that will enhance ionization in the conductance layer most efficiently, with higher- and lower-energy electrons ionizing below or above the conductance layer, respectively. Enhancements in the precipitating particle fluxes, on the other hand, amplify the degree of ionization in the altitude regime where particles of a specified energy are deposited. In fact, the electron density in auroral precipitation regions is proportional to the square root of the energy flux, and consequently the conductance is also approximately proportional to the square root of the energy flux (e.g., Millward *et al.*, 2002; Müller-Wodarg *et al.*, 2012). Therefore, any temporal variations in the precipitating energy flux will be closely tracked by corresponding variations in the ionospheric electrical conductance, though with a delay that depends on the chemical timescales within the conductance layers (Galand *et al.*, 2011).

8.3.1 Solar-wind interactions

Auroral emission on the Earth is driven by the interaction between the Earth's magnetic field and the solar wind, which, in turn, is dominated by a process known as reconnection. Reconnection occurs when two plasmas with non-parallel frozen-in magnetic fields are pushed together. This is visualized as if magnetic field lines from each plasma "break" to "reconnect" with each other, magnetically linking the plasma regions. On Earth, magnetic field lines within the magnetosphere reconnect with field lines carried within the solar wind along the noon edge of the magnetosphere, opening field lines in Earth's polar region to the solar wind (cf., Ch. 10 of Vol. I). This open flux is carried across Earth's polar cap with the solar wind, to the nightside. On the nightside of the polar cap, open field lines are closed and removed from the equatorial plane of the tail by reconnection, at times associated with substorm formation. As these field lines are closed, the polar cap contracts and flows redistribute flux and plasma within the polar regions. These processes drive a twin-cell ionospheric convection pattern, with antisunward flow across the poles, and sunward flows around the equatorward edge of the polar cap (Dungey, 1961; see Fig. 10.5 in Vol. I).

This process is complicated at the giant planets (cf., Ch. 13 in Vol. I), as the scale of the magnetospheres of these planets is significantly larger (as a result of both stronger magnetic fields and weaker solar wind) and the planets rotate more quickly, so that the solar wind takes many planetary rotations to cross the magnetosphere. For example, at Saturn this results in a rotationally dominated

Dungey cycle, where rotating components are stronger than the twin-cell flows, such that a single-cell flow occurs across the polar region, with a return flow only occurring on the dawnside of the planet (see discussion surrounding Fig. 9.5 of Gombosi *et al.*, 2009). Ionospheric flows produce an ionospheric current system that drives current along magnetic field lines, with downward currents on open field lines just poleward of the main aurora, and associated diffuse upward currents near the pole. Equatorward of this, a narrow ring of upward current exists on closed field lines which, in turn, close at lower latitudes. This upward current is directly related to the downward flow of accelerated electrons, driving the main auroral emission at Saturn. As the rotation of the planet drives the ionospheric flows onto the dawnside of the polar region, this results in a dawn enhancement in the auroral emission.

The extent of solar-wind interaction with Jupiter's auroral region remains a matter of significant scientific debate. Ionospheric flows within the dawnside of Jupiter's polar region are clearly held in the solar-wind reference frame, resulting in a strong ionospheric flow relative to the neutral atmosphere (Stallard, 2003). Some have suggested this flow results from a modified Dungey cycle flow similar to that seen at Saturn (Cowley *et al.*, 2003). Although this hypothesis matches with many of the observed conditions within this region, one of the major problems with this interpretation is that Jupiter's dawn polar region sees significant variable auroral emission in a region that might be expected to be free of plasma (Grodent *et al.*, 2003). An alternative explanation for how such "Swirl emission" can exist is that the ionospheric flows observed are driven by solar-wind-driven magnetospheric flows caused by viscous processes at the magnetopause boundary (Delamere and Bagenal, 2010). This hypothesis allows closed field lines, filled with plasma that can produce "Swirl" aurora, to drive flows within the ionosphere that are held within the solar-wind reference frame. Which of these hypotheses actually dominates solar-wind interaction at Jupiter is hotly contested.

Observations of UV auroral emissions from Uranus (Lamy *et al.*, 2012) have shown that these weak auroral emissions are associated with changes in the solar-wind density. The lack of a strong response to solar-wind compressions may reflect the lack of a well-developed tail structure, which would be expected for Uranus' current equinox configuration (e.g., Tóth *et al.*, 2004). This contrasts with Uranus at solstice, when open flux could be produced continuously and flow in the slowly rotating nightside tail (cf., Vol. I, Ch. 13, Fig. 13.9; Cowley, 2013).

8.3.2 Internal current systems

The magnetospheres of both Jupiter and Saturn differ significantly from that of the Earth in the distribution and quantity of plasma contained within them. The

major source of internal plasma at Earth is its ionosphere. As a result, plasma is concentrated very close to the planet, and is mostly found on magnetic field lines close to the planet. Both Jupiter and Saturn have significant sources of plasma away from the planet. At Jupiter, the volcanic moon Io contributes ~1000 kg/s of mass to a torus of equatorially bound plasma that orbits Jupiter close to Io's orbit, at 6 R_J (Dessler, 1980). This torus is by far the dominant source of all plasma within the magnetosphere, with ionized material forming a significant plasmasheet that extends from Io outwards. Saturn has a wider distribution of plasma sources, including the rings close to the planet, the cryovolcanic water plume from Enceladus at 3.95 R_S, as well as scattering from the surfaces of various moons. This results in the concentration of significant plasma in the equatorial regions of both planetary magnetospheres. Because this plasma is generated from neutral material orbiting with Keplerian velocities, it has a nonzero velocity relative to the magnetic field of the planet, which rotates with the planet's interior. In a collisionless MHD approximation of this process, the plasma is frozen into the magnetic field, and the deviation from the planet's rotation rate results in the magnetic field lines being azimuthally bent back near the equatorial plane, driving a radial current outwards through the plasmasheet. This produces a current that closes by producing an equatorward current within the ionosphere as well as field-aligned currents into and out of the ionosphere. In the rotation-dominated magnetospheres of Jupiter and Saturn, the equatorial plasmasheet rotates with the planet on a time scale of ~10 h while small-scale, diffusive interchange of magnetic flux tubes leads to net radial transport of mass outwards and return of magnetic flux inwards on time scales of tens of days (Vol. I, Ch. 13). However, the frozen-field approximation breaks down in the ionosphere of the planet, as charged particles within the ionosphere are accelerated by the surrounding neutral atmosphere. This results in currents that transfer angular momentum from the neutral atmosphere out to plasma within the magnetosphere, producing a steady-state coupling between the atmosphere and magnetosphere that drives magnetospheric plasma into co-rotation with the planet.

There are two limiting factors to this current system.

(i) The Keplerian orbital velocity decreases with distance from the planet, so that maintaining co-rotation requires larger forces. At the same time, the magnetic field strength also decreases with distance, requiring a greater current. As a result, the currents required to maintain co-rotation within the magnetosphere increase with distance from the planet.

(ii) The ionospheric Pedersen conductance represents particle mobility within the ionosphere, parallel to the electric field and perpendicular to the magnetic

field. Because the Pedersen conductivity is finite, the magnitudes of the currents that flow through the ionosphere depend on the conductivity for a given ionospheric electric field. When the current required by the above process grows too large, the force produced begins to make the ionosphere sub-rotate relative the surrounding atmosphere, which in turn allows plasma within the magnetosphere to no longer co-rotate with the planet.

Therefore, as magnetospheric plasma moves radially outwards (a radial flow that occurs as the direct result of charged particles being accelerated away from their Keplerian orbital velocity), the ionospheric Pedersen conductivity required to maintain that plasma's co-rotation in the magnetosphere continually increases. Ultimately, the drifting plasma reaches a tipping point at which ionospheric currents are no longer able to maintain co-rotation, and the plasma begins to rotate significantly slower than the magnetic field of the planet. This nonzero azimuthal plasma velocity results in currents that flow radially outwards through the plasmasheet within the equatorial magnetosphere. This current again closes along magnetic field lines into the ionosphere, producing broader downward currents and ion precipitation in the poleward mapping of this breakdown in co-rotation, and a narrow region of upward currents and electron precipitation just equatorward of the boundary of sub-rotating magnetospheric plasma.

At Jupiter, this breakdown in co-rotation drives a continuous bright main auroral emission (Cowley and Bunce, 2001; cf., Fig. 13.7 in Vol. I) and results in a significant sub-rotational ion wind flow, ~1.5 km/s, in the region of the main emission, caused by Hall drift from the Pedersen currents that drive the aurora (Rego *et al.*, 2000; Stallard *et al.*, 2001). At Saturn, the magnetosphere is significantly more mass-loaded than Jupiter, due to the weaker magnetic field (Vasyliūnas, 2008), and so the breakdown in co-rotation occurs at $\sim 3 R_S$, inside the orbit of Enceladus. The resultant aurora produced by this process at Saturn has been shown to be far weaker (Cowley and Bunce, 2003) and has thus far not been observed in UV emission, but may have been seen in the IR (Stallard *et al.*, 2008, 2010).

This transfer of energy from within the magnetosphere down into the upper atmosphere is universal to any planet with a significant source of plasma within the magnetosphere. This process has been suggested as the potential future source of detectable auroral emission from exoplanets, with strong radio emission resulting from a higher planetary rotation rate (and a presumably stronger magnetic field), and a higher stellar XUV luminosity. Similar current systems have also been suggested as the possible source of already observed radio emission from brown-dwarf stars (Schrijver, 2009; Nichols *et al.*, 2012).

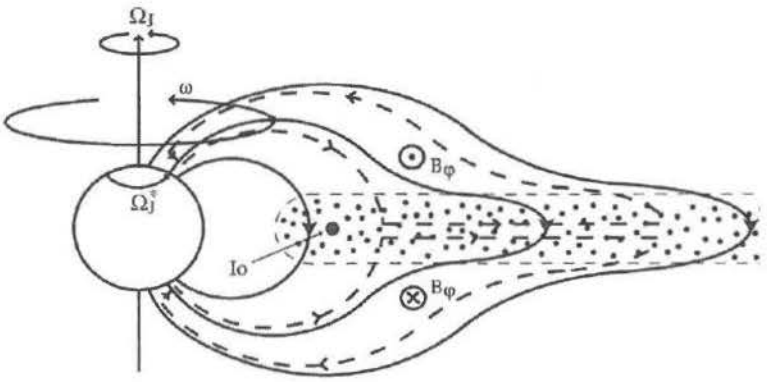

Fig. 8.6 Sketch of a meridian cross section through the Jovian magnetosphere, showing the principal features of the inner and middle magnetosphere regions. The arrowed solid lines indicate magnetic field lines, which are distended outwards in the middle magnetosphere region by azimuthal currents in the plasmasheet. The plasmasheet plasma originates mainly at Io, which orbits in the inner magnetosphere at 6 R_J, liberating $\sim 10^3$ kg s^{-1} of sulphur and oxygen plasma. This plasma is shown by the dotted region, which rotates rapidly with the planetary field due to magnetosphere–ionosphere coupling, while more slowly diffusing outwards. Three separate angular velocities associated with this coupling are indicated. These are the angular velocity of the planet Ω_J, the angular velocity of a particular shell of field lines ω, and the angular velocity of the neutral upper atmosphere in the Pedersen layer of the ionosphere, Ω_I^*. The latter is expected to lie between ω and Ω_J because of the frictional torque on the atmosphere due to ion–neutral collisions. The oppositely directed frictional torque on the magnetospheric flux tubes is communicated by the current system indicated by the arrowed dashed lines, shown here for the case of sub-co-rotation of the plasma (i.e., $\omega \leq \Omega_J$). This current system bends the field lines out of meridian planes, associated with azimuthal field components B_ϕ as shown. (From Cowley and Bunce, 2001.)

A sample sketch of the Jovian magnetospheric current systems is given in Fig. 8.6.

8.3.3 Vasyliūnas cycle

Plasma is continually added to the magnetospheres of both Jupiter and Saturn. Plasma confined to the equatorial region is transported radially outwards (via centrifugally driven flux tube interchange), it is ultimately lost from the magnetosphere through the tail, resulting in a downtail outflow of magnetic field lines that are stretched out and eventually pinched off. This forms a plasmoid, containing trapped closed field lines and released downtail, as well as closed, relatively empty field lines that propagate back onto the dayside of their magnetosphere, a process described as the Vasyliūnas cycle (Vasyliūnas, 1983). The relatively few particles on the closed flux tubes are accelerated as the flux tube springs

back to a more dipole configuration on releasing the plasmoid. This process has been invoked to explain the region of bright auroral emission in the duskside of Jupiter's polar region, often leading to bright polar flare emission (Grodent *et al.*, 2003).

8.3.4 Moon–magnetosphere–atmosphere interaction

Giant planets also have aurorae directly related to the magnetic interaction between the magnetosphere and moons. These auroral emission fall into two types, a spot of emission located within the planetary ionosphere at the magnetically mapped position of the moon itself, and a tail of emission that extends away from the moon, mapping to the moon's orbital path (e.g., Kivelson *et al.*, 2004). The localized moon spots are created by the Alfvénic disturbance imposed by the moon upon the magnetic flux tube sweeping past the moon and accelerating electrons in both directions along the field lines (Bonfond *et al.*, 2008). Such spot emission was first identified for Io at Jupiter (Connerney *et al.*, 1993), but similar spot features have now been identified for Europa, Callisto, and Ganymede at Jupiter (Clarke *et al.*, 2002, 2011), and for Enceladus at Saturn (Pryor *et al.*, 2011). The trailing emission, seen in the wake of both Io (Clarke *et al.*, 2002) and Europa (Grodent *et al.*, 2006), represents a steady state current system which accelerates localized plasma from the moon into co-rotation with the surrounding magnetic field. At Saturn, a weak H_3^+ emission aurora is observed at latitudes that map magnetically to between 3–4 R_S, extending around the entire planet. This aurora might be considered a proxy for Jupiter's breakdown in co-rotation aurora, but because mass loading means plasma from Enceladus is never fully accelerated into co-rotation, it might equally be described as a satellite wake emission that extends to all longitudes in the ionosphere (Stallard *et al.*, 2008, 2010).

8.3.5 Additional magnetosphere–atmosphere interaction

Charged particles that are not part of a current system within a magnetosphere tend to be confined near the equatorial plane, through magnetic mirroring, because particles propagating up the field line towards the planet receive a repulsive force due to the increased magnetic field strength along the field line, leading to a bounce motion between the magnetic poles. However, if the particles are energetic enough, or if their pitch angles small enough, the magnetic mirror points of the particles can extend into the atmosphere, precipitating the particles into the atmosphere. While this process produces aurorae, both the particle energies and the total flux of the precipitating particles are typically smaller than those corresponding to discrete aurora, resulting in weaker and more diffuse emission. This precipitation process

will also vary if the magnetic field strength varies with longitude, resulting in longitudinal enhancements in precipitation.

At Jupiter, this form of aurora has been suggested as one source of the mid-to-low latitude emission (Miller *et al.*, 1997), and the radiation belt has been modeled as a possible source for both H_3^+ and X-ray emission (Abel and Thorne, 2003). At Saturn, hot plasma located between 8–15 R_S has been suggested as a source of an auroral arc observed in both IR and UV on the nightside of the planet, equatorward of the main oval (Grodent *et al.*, 2010). In addition, observations of the equatorial region of the planet have shown variations in the H_3^+ emission at latitudes that magnetically map to Saturn's rings (O'Donoghue *et al.*, 2013). It is likely that ionized water group particles are entering Saturn's ionosphere along magnetic field lines, leading to reductions in the local electron density, and in turn resulting in an increase in the corresponding H_3^+ density (Moore *et al.*, 2015).

8.4 Auroral emissions

Within the auroral region, field-aligned currents drive particle precipitation into the atmosphere, ultimately driving a variety of auroral emissions. The sources for this auroral power come from two major types of precipitation: discrete aurorae are formed from precipitating charged particles that have been accelerated into the atmosphere along magnetic field lines, while diffuse aurora is formed from energetic precipitating particles resulting from plasma interaction in the magnetosphere. Aurorae are produced through energy released by precipitating energetic particles in their interaction with an atmosphere. At the giant planets, auroral emissions are produced in four different ways: emission can be released directly from the precipitating particle itself; the precipitation process can transfer energy into the atmosphere, resulting in either the energetic excitation or the ionization of the atoms or molecules within the atmosphere; and the precipitation process heats the atmosphere both directly and indirectly, leading to a thermalized auroral emission from the atmosphere. Auroral emissions from the giant planets are discussed in detail within Bhardwaj and Gladstone (2000), Kurth *et al.* (2009), and Clarke *et al.* (2004). In addition, an overview of Jupiter's magnetosphere and auroral processes is given by Bagenal *et al.* (2014). Figure 8.7 shows a representative comparison between the UV and IR aurora at Jupiter, with major features indicated.

8.4.1 Emission from precipitating particles

Radio and X-ray emissions are produced directly from the precipitating particle itself. Radio emission is generated by precipitating electrons as they are accelerated into the atmosphere along the magnetic field lines. They are thought to be produced

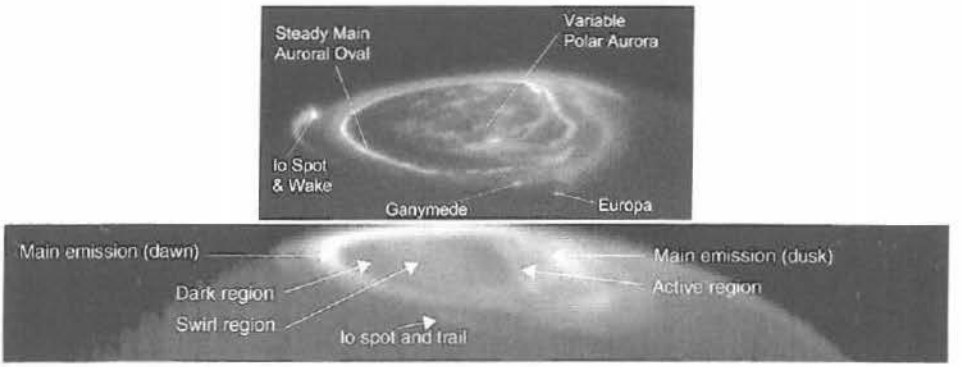

Fig. 8.7 UV (top) and IR (bottom) auroral images of Jupiter, with major features indicated. (Top image from Ch. 13 in Vol. I (Clarke *et al.*, 2004); bottom image from T. Stallard, personal communication, 2014.)

by cyclotron maser instabilities, which rely on the motion of energetic electrons around the magnetic field and produce a resonant radio emission. Because such instabilities require very-high-energy electrons, radio aurorae appear to originate in the low-density region above the planet, where potential differentials along field lines significantly increase the mean energy of electrons. This is the cause of the significant auroral radio emission observed at all the giant planets (Zarka, 1998; Lamy *et al.*, 2009).

At Earth, auroral X-ray emission is produced most commonly by bremsstrahlung resulting from high-energy precipitating electrons scattered by the atmosphere. At Jupiter, X-ray bremsstrahlung is present and overlaps spatially with the bright auroral oval seen in the UV, also induced by energetic electrons (e.g., Branduardi-Raymont *et al.*, 2007). However, the majority of the observed X-rays are too energetic to have been produced by such a process (Metzger *et al.*, 1983). Instead, they result from precipitating energetic heavy ions, which have become highly charged through electron stripping by interaction with atmospheric neutrals and can subsequently undergo charge-exchange (i.e., electron capture) through further collisions, leading to emission of an X-ray photon associated with K-shell lines. The production of Jovian X-rays by precipitating ions is a process identified by spectroscopy (Branduardi-Raymont *et al.*, 2007) and by the location of a hot spot of X-ray emission poleward of the main auroral emission (Branduardi-Raymont *et al.*, 2008), at a location that is thought to map to downward currents (Gladstone *et al.*, 2002).

8.4.2 Atmospheric excitation

Particle precipitation leads to significant excitation of the underlying atmosphere, in turn producing prompt emission from excited molecules and atoms. It is

this process that dominates the auroral emission seen on Earth, and though the atmospheric composition is significantly different, similar aurorae are observed on the giant planets. These auroral emissions are directly controlled by the precipitation process and, as such, provide an instantaneous view of the particle precipitation process. The composition of the upper atmospheres of giant planets is dominated by hydrogen, and so the observed prompt emission is largely due to hydrogen excitation. The brightest prompt emission from giant planets is associated with the excitation of hydrogen atoms (already present in the atmosphere or produced from the dissociation of H_2), resulting in the strong UV Lyman-α emission (at 121.6 nm) and, to a lesser extent, visible light Balmer series emission (including lines at 410.2, 434.1, 486.1, and 656.3 nm; Dyudina *et al.*, 2011). There are also significant emissions from molecular H_2, produced by electronically excited hydrogen molecules in the Lyman and Werner bands (dominating over ~90–170 nm), and a weak continuum emission from the H_2 a-b dissociation transitions (200–250 nm). Hydrogen may also be electronically excited by the Sun, with some evidence of solar fluorescence (Shemansky *et al.*, 1985), though the observed transitions may also be caused by scattering of sunlight (Yelle *et al.*, 1987). Vibrational excitation of hydrogen also produces infrared H_2 quadrupole emission, but under most ionospheric conditions these molecules are thermalized, and so evidence of such excitation is lost. However, excitation within the collisionless exosphere, at the top the atmosphere, is not removed by thermalization, and so IR excitation aurora caused by cold electrons may occur in this rarefied region (Hallett *et al.*, 2005).

8.4.3 Thermal auroral emission

Molecules produce thermalized auroral emission wherever the atmosphere is heated through the interaction between the atmosphere and the magnetosphere, as long as the spontaneous emission time scale is significantly longer than the time scale for collisions (otherwise local thermal equilibrium is lost). Molecular hydrogen, hydrocarbons, and hydrogen ions all emit infrared light when thermalized within the surrounding neutral atmosphere, with this emission representing one of the major energy sinks for the upper atmosphere (Drossart *et al.*, 1993). Observations of this energy loss process have concentrated upon cooling from the H_3^+ molecule, as this is the most easily observed of the thermalized auroral emitters in giant-planet atmospheres. These observations have shown that auroral H_3^+ is hotter than H_3^+ in non-auroral regions (Lam *et al.*, 1997; Stallard *et al.*, 2002), though exact measurements of the local temperature can be difficult, as changes in observed temperature are at least partially driven by changes in the source altitude,

combined with the heat gradient; sudden changes in temperature may be due to changes in the H_3^+ peak altitude, rather than the actual temperature of the neutral atmosphere (Lystrup *et al.*, 2008).

Although observations have concentrated on H_3^+, it is the underlying hydrocarbon molecules that produce the majority of cooling within the upper atmospheres. However, observations of the heat produced within these molecules has not progressed significantly since early measurements on Jupiter, which showed an auroral hot spot at ~60° N and 180° W (Caldwell *et al.*, 1980; Livengood *et al.*, 1990), with temperatures of ~250–320 K at 2–34 microbar (Kostiuk *et al.*, 1993). Quadrupole H_2 auroral emission contributes relatively little to the overall cooling of the atmospheres of giant planets, but provides a measure of temperatures in a layer somewhere between that of high-altitude H_3^+ and low-altitude hydrocarbons. On Jupiter, they emit at a few microbar and have temperatures not inconsistent with those found for H_3^+ (530–1220 K; Kim *et al.*, 1990).

8.4.4 Ionization aurora

Particle precipitation is the dominant source of ionization within the auroral regions of the gas giants. Because there is significant thermal inertia within the upper atmospheres of giant planets (Müller-Wodarg *et al.*, 2012), any resultant thermalized aurora will vary slowly, both temporally and spatially. However, ionization occurs on much smaller scales, and is only limited by the lifetime of the resultant ions. As a result, aurorae in infrared lines are dominated in structure by the ionization process, while overall brightness across the entire auroral region is more strongly controlled by temperature.

The dominant ionic products caused by particle precipitation depend on where in the atmosphere the peak ionization is occurring. At Jupiter, the peak ionization occurs beneath the homopause, resulting in a significant amount of both hydrogen and hydrocarbon ions being formed. However, because H_3^+ is easily destroyed by neutral hydrocarbons, the H_3^+ density peaks at a higher altitude, above the homopause. At Saturn, the peak ionization occurs above the homopause, so that there are few hydrocarbon ions and H_3^+ becomes a dominant product within the auroral ionosphere.

Infrared emission from these molecules is dominated by temperature changes. However, because this temperature varies over long temporal and spatial time scales, the localized H_3^+ auroral morphology is controlled by the density of H_3^+, which in turn is controlled by the particle precipitation process (Stallard *et al.*, 2001). An H_3^+ aurora thus closely follows the morphology seen within prompt UV emission, with particle precipitation driving ionization in the same location as

hydrogen excitation. The main auroral differences come from precipitation energy, where UV aurorae are formed beneath the homopause at Jupiter; short-time-scale effects, where the ~10–15 min recombination rate of H_3^+ smooths out short-term changes in precipitation; and localized heating, where strong thermal gradients can actually influence localized intensity variations (Clarke *et al.*, 2004; Radioti *et al.*, 2013).